POLITECNICO DI TORINO
Repository ISTITUZIONALE

Hydraulic Brake Systems for Electrified Road Vehicles: A Down-sizing Approach

Original
Hydraulic Brake Systems for Electrified Road Vehicles: A Down-sizing Approach / Anselma, P.G., Belingardi, G.. - (2020), pp. 1-9. (Eurobrake 2020) [10.46720/eb2020-ibc-024].

Availability:
This version is available at: 11583/2859173 since: 2020-12-29T10:27:43Z

Publisher:
FISITA

Published
DOI:10.46720/eb2020-ibc-024

Terms of use:

This article is made available under terms and conditions as specified in the corresponding bibliographic description in the repository

Publisher copyright

(Article begins on next page)

14 September 2026

Hydraulic Brake Systems for Electrified Road Vehicles : a Down-sizing approach

Pier Giuseppe Anselma*, Giovanni Belingardi

Department of Mechanical and Aerospace Engineering (DIMEAS),
Center for Automotive Research and Sustainable Mobility (CARS),
Politecnico di Torino, Torino, Italy

https://doi.org/10.4672/EB2020-IBC-024

ABSTRACT: Down-sizing hydraulic brake systems can is made possible in electrified road vehicles thanks to the braking torque contribution provided by electric machines. Benefits in terms of weight and cost of the system can be ensured in this way. Nevertheless, appropriate care should be taken not to excessively deteriorate the overall electrical energy recovery capability of the electrified vehicle during braking maneuvers. For this reason, a multi-target optimization framework is developed in this paper to down-size hydraulic brake systems for electrified road vehicles while simultaneously maximizing the braking energy recovery capability of the electrified powertrain. Firstly, hydraulic brake system, electrified powertrain and vehicle chassis are modeled in a dedicated simulation platform. Subsequently, particle-swarm optimization is employed as search algorithm to identify optimal sizing parameters for the hydraulic brake system. Sizing variables particularly include diameter and stroke of the master cylinder, electrically assisted booster diameter, front brake piston diameter and rear brake piston diameter. The simulation of homologation tests for safety standards ensures that retained combinations of sizing parameters complies with regulatory requirements. A case study proves that the developed methodology is flexible and effective at rapidly producing several sub-optimal sizing options for both front-wheel drive and rear-wheel drive layouts for a retained battery electric vehicle.

KEY WORDS: Computer-aided engineering, electric vehicles, hydraulic brake systems, optimal down-sizing, safety standards

1. Introduction

Electrification of road vehicle powertrains is currently emerging as a global trend in automotive industry [1]. This transformation does not affect powertrain systems solely [2][3], yet it entails revolutions in the remaining vehicular elements as well [4]. In this framework, new research trends have recently arisen in the field of braking concerning the optimal control of regenerative braking and the optimal re-sizing of hydraulic brake systems for electrified vehicles. Regarding optimal control of regenerative and hydraulic braking for battery electric vehicles (BEVs), Zhang et al. in 2012 assessed different control strategies such as maximum-regeneration-efficiency, good-pedal-feel and coordination [5]. In 2014, Junzhi et al. developed a cooperative braking control strategy for a rear-wheel-drive electrified minivan considering both recovered energy and comfort [6]. In 2015, Kumar and Subramanian proposed a combined braking strategy for a series hybrid electric vehicle layout [7].

Despite the optimal control of regenerative and hydraulic braking is being adequately assessed in literature, few works have been presented regarding optimal design and sizing of hydraulic brake systems for electrified road vehicles. Nevertheless, thanks to the regenerative braking torque provided by the electrical powertrain, opportunities are offered in down-sizing the components of current hydraulic brake systems to save weight and cost and to allow them operating at enhanced efficiency. As example, in 2017 Hall experimentally compared real-world daily braking events in Los Angeles considering both a conventional vehicle (CV), i.e. embedding an internal combustion engine solely and a BEV exhibiting similar size and mass. Obtained results suggested that, by adopting BEVs rather than CVs, both the number of braking events and the overall amount of energy dissipated by the friction brakes could be decreased by factors of 8 and 20, respectively [8]. In 2018, Shenberger and Antanaitis numerically investigated the conversion of a production mid-size sedan to a BEV and proposed a heuristic approach to down-size the hydraulic brake system for the BEV. According to results, consistent mass reduction for both the caliper assemblies and the rotors could be achieved for the BEV while simultaneously guaranteeing similar braking performance compared with the CV layout. Nevertheless, following this approach, the obtained brake system parameters were not guaranteed being the optimal ones. Moreover, the illustrated methodology did not consider down-sizing some fundamental components of a hydraulic brake system such as the master cylinder and the brake booster [8].

For the sake of filling the outlined research gaps, this work proposes a straightforward computer-aided engineering (CAE) methodology to optimally downsize the components of hydraulic brake systems for electrified road vehicles. The design methodology illustrated particularly takes inspiration from the work originally presented by the authors in 2017 in which a rapid heuristic design approach was presented for hydraulic brake systems of CVs [9]. This first work was then broadened up in 2019 by the authors of this papers by including a brute force optimization

framework for the brake system layout [11]. In this paper, several improvements can be defined for the proposed CAE methodology for hydraulic brake systems:

- The design approach originally illustrated for CVs is extended to hydraulic brake system layouts for electrified road vehicles;
- An increase in the fidelity level for hydraulic brake system, vehicle and powertrain numerical models is achieved by employing a dedicated simulation software;
- A refinement for the optimization approach is accomplished by implementing a consolidated and efficient design space exploration method from literature.

Multiple optimization targets are considered here when downsizing the hydraulic brake system such as the averaged size of components and the electrical energy recovered in specific braking maneuvers. The rest of this paper is organized as follows: numerical models for the hydraulic brake system, the vehicle chassis and the electrified powertrain are described. The implemented CAE approach for designing and sizing hydraulic brake systems of electrified road vehicles is then presented and detailed. Next, a case study is presented in which the hydraulic brake system is optimally sized for a BEV layout considering both front-wheel-drive (FWD) and rear-wheel-drive (RWD) cases. Conclusions are finally given.

2. Modeling approach

In this section, numerical models for the BEV powertrain, chassis and hydraulic brake system are outlined. In general, these models find implementation in Amesim® software as displayed in Figure 1 and detailed below.

2.1. Hydraulic brake system for electrified road vehicles

Figure 2 displays a schematic diagram of a hydraulic brake system for electrified road vehicles. Three main sub-system can be identified by the brake pressure generation, the brake pressure distribution and the brake pressure to friction conversions. These sub-systems will be detailly described in the following up of this paragraph.

2.1.1. Brake pressure generation

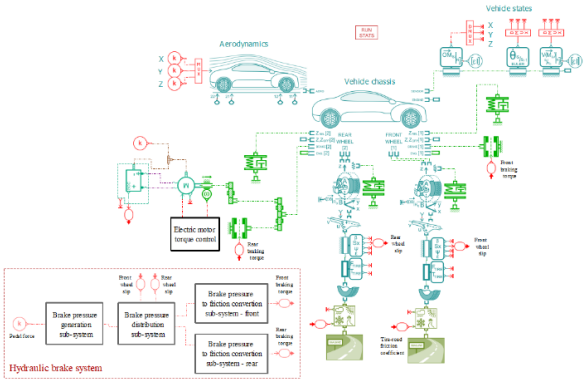

Figure 1 The BEV and hydraulic brake system model implemented in Amesim®

The foot pedal force applied on the brake pedal and the brake line pressure in turn generated by the master cylinder represent the input and the output for this subsystem, respectively. The analytical relationship between the generated brake line pressure p_{line} and the foot force applied to the pedal is expressed in equation (1):

$$p_{line} = \frac{F_{pedal} \cdot l_{pedal} \cdot \eta_{pedal} \cdot r_{boost}}{A_{MC}} \quad (1)$$

where l_{pedal} and η_{pedal} respectively represent lever ratio and efficiency of the brake pedal. r_{boost} is the boosting ratio achieved thanks to the employment of a dedicated brake booster, while A_{MC} stands for the cross-sectional area of the plunger linked to the brake pedal. l_{pedal} relates to the pedal mechanical connection and regulates the relationship between the pedal travel and the master cylinder stroke as in equation (2):

$$l_{pedal} = \frac{x_{pedal}}{(st_{MC} - cl_{MC})} \quad (2)$$

where x_{pedal} represents the maximum achievable pedal travel (generally established according to packaging constraints), while st_{MC} and cl_{MC} stand for the master cylinder stroke and clearance, respectively.

In BEVs, given the absence of an internal combustion engine, the enhancement of the force applied to the brake pedal is usually not achieved by means of a vacuum-assisted booster as in CVs. Rather, a primary piston (identified with the cross-sectional area A_{boost} in Figure 2) is linked to a ball screw mechanism powered by an electric motor [12]. When the position of the plunger changes due to the applied foot pedal force, the brake-boost controller adjusts the position of the primary piston parallelly using the motor connected to the ball screw. As a result, r_{boost} can be defined in terms of the cross-sectional areas of the plunger (A_{MC}) and the primary piston (A_{boost}) as in equation (3).

$$r_{boost} = \frac{A_{MC} + A_{boost}}{A_{MC}} \quad (3)$$

2.1.2. Brake pressure distribution

Adjusting the line pressure between front and rear brakes represents the main scope of the electronic brake distribution (EBD) system. A reduction in the line pressure for the rear axle circuit is particularly achieved by means of hydraulic valves coordinated by an appropriate control strategy. Following a commonly adopted approach, the EBD system operates here according to an 'equal slips' strategy in which the brake force distribution is regulated so that rear wheels and front wheels exhibit equal values of longitudinal slip [13]. A proportional–integral–derivative (PID) controller is particularly implemented in the brake pressure distribution block in Figure 1 taking as input the difference between

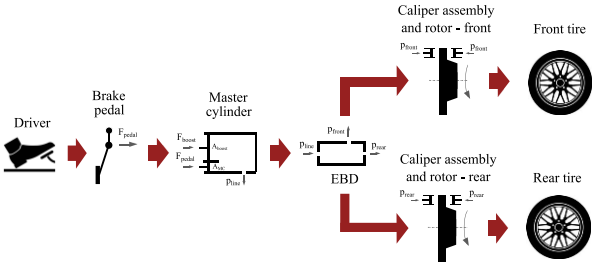

Figure 2 Schematic diagram of a hydraulic brake system for electrified road vehicles

the slip values at front and rear brakes and being responsible for reducing the line pressure at the rear brakes accordingly.

2.1.3. Brake pressure to friction conversion

The generated line pressure can be finally converted into friction energy by means of brake pistons, calipers and rotors, thus reducing the kinetic energy of the vehicle and decelerate it. The relationship between the line pressure and the generated brake torque for a single wheel ($T_{brake_{wheel}}$) is particularly proportional to the brake gain factor $gain_{brake}$ as reported in equation (4) [11].

$$gain_{brake} = \frac{T_{brake_{wheel}}}{p_{line}} = 2 \cdot A_{BP} \cdot \mu_{pad} \cdot (r_{rotor} - r_{BP} - cl_{BP}) \cdot \eta_{thermal}(T) \quad (4)$$

A_{BP} and μ_{pad} represent the brake piston area and the brake pad coefficient of friction, respectively. r_{rotor} and r_{BP} are the radii of the brake rotor and the brake piston, respectively. cl_{BP} is the brake piston to the rotor edge clearance, while $\eta_{thermal}$ represents the thermal efficiency as a function of the rotor temperature T.

Here, the numerical approach to evaluate the rotor temperature is retained from the user manual of CarSim® software and followingly detailed [14]. All the mentioned experimental 1D lookup tables are retained from CarSim® as well with reference to the brake system for an A-segment city car. The brake rotor temperature at the generic time instant *i* can be evaluated from its value at the previous time instant *(i-1)* following equation (5).

$$T_i = T_{i-1} + \frac{\int_{t_{i-1}}^{t_i}(P_{in} - P_{out})}{M_{rotor} \cdot c_p(T)} \quad (5)$$

M_{rotor} and c_p stand for rotor mass and specific heat as an empirical function of the rotor temperature, respectively. P_{in} and P_{out} represent the power input from the brake operation and the dissipated power output by cooling, respectively. The energy flux input to the rotor, which causes a certain temperature variation between two adjacent time instants, can be obtained by integrating the net input power between the considered time instants. The power input P_{in} can specifically be calculated by multiplying the wheel brake torque by the wheel speed ω_{wheel} in equation (6).

$$P_{in} = T_{brake_{wheel}} \cdot \omega_{wheel} \quad (6)$$

On the other hand, the power removed by the cooling effects P_{out} can be calculated from equation (7):

$$P_{out} = c(V_x) \cdot M_{rotor} \cdot c_p(T) \cdot (T - T_{air}) \quad (7)$$

where c represent the coefficient for rotor cooling by air circulation as an empirical function of the vehicle longitudinal speed V_x, while T_{air} is the external air temperature. The thermal efficiency and the resulting brake torque can be computed for each wheel of the vehicle in this way.

2.2. BEV modelling

In this sub-section, numerical models for both the BEV powertrain and chassis will be presented.

2.2.1. BEV powertrain

As displayed in Figure 1, the BEV powertrain layout retained here consists of an electric motor (EM) linked to the driven axle by means of a direct drive transmission. In this way, the angular speed of the EM is proportionally linked to the angular speed of the driven wheels by means of the direct drive transmission ratio. An EM controller is embedded that regulates the EM negative torque T_{EM} as a function of the vehicle speed signal in equation (8):

$$T_{EM} = \begin{cases} T_{regen_{\max}}(\omega_{EM}) & V_x > V_{x_\lim} \\ 0 & V_x \leq V_{x_\lim} \end{cases} \quad (8)$$

where $T_{regen_{\max}}$ represents the minimum achievable value of EM torque as function of the EM angular speed ω_{EM}. $T_{regen_{\max}}$ can particularly be obtained by interpolating in the empirical 1D lookup table related to the retained EM with ω_{EM} as independent variable. As common practice, $V_{x_\lim}$ is retained as cut-off vehicle speed value for the regenerative braking operation. In other words, below $V_{x_\lim}$ only friction braking will be applied to the BEV given the ineffectiveness of the regenerative braking system at low vehicle speed values. A value of $V_{x_\lim}$ of 10 km/h is retained here from [15]. Furthermore, a PID controller is included that reduces the absolute value of the negative torque operated by the EM in case an excessive value of longitudinal slip is reached by the driven wheels during braking events [16].

Once ω_{EM} and T_{EM} are determined, the value of the EM electrical efficiency η_{EM} can be computed from an experimental 2D lookup table with torque and speed as independent variables. Finally, the charged battery energy E_{batt} throughout the braking maneuver can be determined by integrating the battery electrical charging power following equation (9).

$$E_{batt} = \int_{t_0}^{t_f}(T_{EM} \cdot \omega_{EM}) \cdot \eta_{EM} \cdot \eta_{batt}\ dt \quad (9)$$

η_{batt} represents the battery electrical efficiency which can be evaluated at each time instant by means of an equivalent circuit model. More detailed about the retained battery modelling approach for BEVs can be found in [17].

2.2.2. Vehicle chassis

As it can be noticed from Figure 1, the vehicle chassis is modelled in this paper considering a 7 degrees of freedom (DoFs) model. Retained degrees of freedom are particularly the following ones:

- Absolute displacement of the center of gravity (CoG) of the vehicle body on the longitudinal axis;
- Absolute displacement of the CoG of the vehicle body on the vertical axis;
- Pitch angle of the vehicle body;
- Vertical lift of the front axle spindle;
- Vertical lift of the rear axle spindle;
- Relative rotation angle between wheel and spindle of the front axle;
- Relative rotation angle between wheel and spindle of the rear axle.

The 7 DoFs numerical chassis model has been selected in this case for assessing BEV braking maneuvers as a reasonable trade-off in terms of enhanced fidelity level and computational light-weighting. Indeed, it allows capturing higher order dynamics compared to the 3 DoFs model previously retained by the authors in [9]. At the same time, since the maneuvers selected from safety standards and simulated in this paper consider straight line braking solely, the 7

DoFs chassis modelling approach allows maintaining computational advantage compared to more detailed modelling approaches (e.g. 15 DoFs model) that consider lateral vehicle dynamics as well. In this case, a single wheel is modelled per each axle, and numerical values for its variables are doubled when interfacing with the vehicle body. As far as the braking torque is concerned, both regenerative torque and friction torque are considered for the wheels of the driven axle, while only friction braking torque is retained for the non-driven axle. Finally, the tire-road interface is modelled according to the well-established Pacejka formulation [18].

3. Developed CAE Methodology

In this section, the developed CAE methodology for designing and sizing hydraulic brake system for electrified road vehicles finds detailed illustration. The overall workflow of the implemented procedure is displayed in figure 3 and described in the follow up of this section. In general, particle swarm optimization (PSO) is adopted here as optimal design exploration algorithm. The following five sizing parameters for the BEV hydraulic brake system layouts are retained:

- Master cylinder diameter (d_{MC})
- Master cylinder stroke (st_{MC})
- Ratio between booster assist primary piston diameter and master cylinder diameter (d_{boost}/d_{MC})
- Front wheels brake piston diameter ($d_{BP_{front}}$)
- Rear wheels brake piston diameter ($d_{BP_{rear}}$)

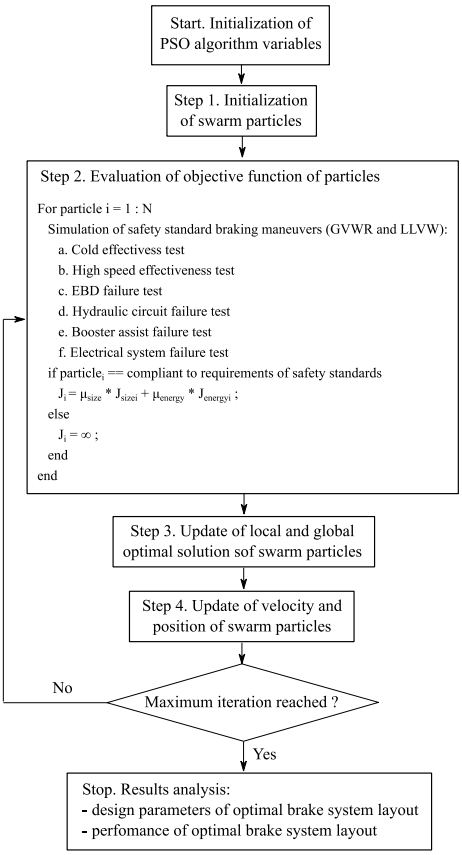

Figure 3 Workflow of the implemented CAE methodology for hydraulic brake systems

The simulation of braking maneuvers from safety standards can then help discriminating whether a set of component sizes can satisfy regulatory requirements. In positive case, a dual-objective evaluation is carried out considering the overall size of the brake system layout and the averaged electrical energy recovered over simulated braking events. The PSO algorithm allows identifying the optimal solution of component sizes according to the retained evaluation criteria. The rest of this section is organized as follows: the retained PSO algorithm is described, while the objective function evaluation of particles (step 2 in figure 3) is subsequently detailed.

3.1. The PSO algorithm

PSO represents a stochastic optimization algorithm based on a simple mathematical model developed by Kennedy and Eberhart in 1995 to describe the social behaviour of birds and fishes [19]. In PSO, a population of N particles (initialised at step 1 in figure 3) explores the space of solutions for the optimization problem aiming at minimizing a given objective function J. The position of particles in the swarm is defined by a vector and updated at each iteration of the algorithm (step 4 in figure 3) according to three main factors:

- inertia: each particle is associated with a velocity vector, which tends to be maintained;
- cognitive factor: each particle tends to move towards its personal best point that has been visited so far;
- social factor: each particle tends to move towards the global best solution of the swarm, i.e. the best point that has been visited so far by the whole set of particles.

PSO is employed in this work due to its capability of efficiently handling global optimization problems characterized by continuous variables. Compared to genetic algorithm (GA) as another popular stochastic optimization algorithm [20], PSO features ease of tuning and management of its parameters, thus enhancing the probability of effectively returning a global optimal solution [21]. Furthermore, few research works can be found in literature concerning the successful application of PSO in the field of brake systems [22] and BEV chassis [23]. In this paper, the PSO algorithm finds implementation in MATLAB® software with reference to the dedicated toolbox provided by the Yarpiz project. The reader interested in obtaining more details concerning the retained mathematical formulation for PSO can consult [24].

Here, the position of a particle identifies specific values of the brake system sizing parameters. During step 2 of the PSO workflow illustrated in figure 3, objective function values for the swarm particles need evaluation. This is performed by following a two-stage procedure: a check is firstly conducted whether the particle (i.e. the brake system layout) under analysis can comply with regulatory requirements, then a value for the objective function is calculated.

3.1.1. Safety standard requirements for hydraulic brake systems

In this work, the two most significant safety homologation standards for light road vehicle hydraulic brake systems are considered, i.e. the "Federal Motor Vehicle Safety Standard No. 135 - Light Vehicle Brake Systems" for the US legislation [25], and the "UNECE Regulation No.13-H" for the EU legislation [26]. Retained homologation tests are listed in Table 1 together with corresponding requirements for stopping distances.

Each test examines straight-line braking and must perform successful for two vehicle loading conditions, i.e. lightly vehicle weight (LLVW) and gross vehicle weight rating (GVWR). GVWR represents the maximum operating weight of the BEV as specified by the manufacture, while LLVW defines unloaded vehicle curb weight with an additional mass of 180 kg (i.e. approximately two people). Other common features for the retained homologation tests are as follows:

- the road-tire friction coefficient is set to 0.9;
- wheel lockup events are not allowed for more than 0.1 seconds;
- the applied brake pedal force is constant throughout each homologation test and it can be picked within the range of 65-500 N.

Tests 1 and 2 retain normal operation for the BEV brake system and they only distinguish by different values of initial speed and stopping distance requirement. A functional failure of the EBD system is considered in Test 3 with rear brake circuits exhibiting the same value of line pressure as the front brake circuits. In test 4, a leakage failure is simulated for the hydraulic circuit. Since two hydraulic sub-circuits are usually installed on road vehicles considering diagonal tires (i.e. front-left and rear-right, front-right and rear-left), only one wheel per axle is considered braking in this case. A functional failure of the booster assist is replicated in Test 5. Finally, a high voltage electrical system failure is considered in Test 6. This corresponds to the electric motor not being capable of providing negative torque to the driven wheels, i.e. only the friction torque contribution provided by the hydraulic brake system is retained. It should be noted that, in this case, the hydraulic brake system alone should comply with the regulatory requirements for the cold effectiveness test.

Each listed safety standard test can thus be simulated considering the numerical model developed in Amesim® software for the hydraulic brake system and the BEV chassis and powertrain. The value of objective function for the retained particle (i.e. brake system sizing candidate) can then be evaluated at the following step.

3.1.2. Objective function evaluation

After each considered safety standard test is simulated in Amesim® software at step 2 in figure 3, the objective function can be assessed for the specific hydraulic brake system sizing candidate. A penalization term is particularly considered for those sizing candidates that do not meet the regulatory requirements. This corresponds, as example, to the simulated stopping distance exceeding the test limit or to a wheel lockup event occurring for more than 0.1 seconds in any of the considered standard tests. In this case, a remarkably large value of objective function (symbolic of infinite) is assigned to the corresponding brake system sizing candidate. On the other hand, if the performance of the retained sizing candidate i complies with all the considered regulatory requirements, its overall objective function is evaluated in equation (10) as a weighted sum of a size cost term and an energy cost term:

Table 1 Safety standard requirements for road vehicle hydraulic brake systems performance aption

	Test name	Initial vehicle speed [km/h]	Stopping distance requirement [m]
1	Cold effectiveness	100	70
2	High speed effectiveness	$0.8 \cdot V_{max}$	$0.1 \cdot V_{max} + 0.0067 \cdot V_{max}^2$
3	EBD failure	100	110
4	Hydraulic circuit failure	100	168
5	Booster assist failure	100	168
6	High voltage electrical system failure	100	70

$$J_i = \mu_{size} \cdot J_{size_i} + \mu_{energy} \cdot J_{energy_i} \quad (10)$$

Where μ_{size} and μ_{energy} represent weighting factors for size and energy cost terms, respectively. In this paper, to evaluate the size cost term, the search range for each of the 5 sizing parameters listed above is initially normalized. In other words, values ranging from 0 to 1 are considered for the search range of each sizing parameter. Minimum value and maximum value of ranges for each sizing parameter are particularly associated to 0 and 1, respectively. Then, an averaged value is calculated considering all the 5 sizing parameters. By minimizing this objective function term, the retained optimization algorithm performs a down-sizing of the overall hydraulic brake system layout. Benefits in terms of weight and cost for the hydraulic brake system could be achieved in this way.

On the other hand, the energy cost term is considered to enhance the electrical energy recovery capability of the BEV during braking maneuvers. It might indeed happen that, due to a high value of line pressure, an excessive friction torque is applied to the driven wheels. In this case, the EM torque controller would need to reduce the regenerative torque to avoid wheel lockup events, thus compromising the electrical energy recovery capability of the electrified powertrain. The minimization of the energy cost term J_{energy_i} is particularly considered here to avoid this drawback. The calculation of J_{energy_i} is performed in equation (11), where $\overline{E_{batt_i}}$ represents the averaged recovered electrical energy by the BEV layout embedding the hydraulic brake system sizing candidate under analysis and considering braking maneuvers of Tests 1 to 5 for both GVWR and LLVW cases.

$$J_{energy_i} = \frac{1}{\overline{E_{batt_i}}} \quad (11)$$

The minimisation of J_{energy_i} thus allows maximizing the recovered electrical energy during retained braking maneuvers.

4. Case study

In this section, a case study is performed to assess the effectiveness of the proposed CAE methodology for hydraulic brake systems of electrified road vehicles. Retained BEV specifications are reported in Table 2 referring to the commercially available Mitsubishi MiEV®, for which a large amount of open-source data are available [27][28]. Concerning EM and battery operational lookup tables, these are retained from data embedded in Amesim® software and appropriately scale to match the numerical values reported in Table 2 [29].

As far as sizing parameters are concerned, retained minimum and maximum values are reported in Table 3. The design space can thus be generated from the combination of values for the listed sizing parameter continuously swept within search boundaries. With reference to the size cost function described in Section 3, each minimum and maximum values shown in Table 3 correspond to 0 and 1 size cost terms for the corresponding sizing parameter, respectively. Particularly for the master cylinder stroke, its minimum and maximum values are retained considering a pedal lever ratio comprised within 3 to 4 to comply with ergonomics constraints [9]. Numerical values for the remining parameters of the hydraulic brake system are retained from [11].

It should be noted that, since the objective function to minimize in equation (10) represents a weighted sum of two optimization targets, a further sweep of the two weighting coefficients μ_{size} and μ_{energy} is needed to obtain the overall multi-objective Pareto frontier of optimal sizing candidates. Here, values for μ_{size} and μ_{energy} are retained so to have their sum equal to 1. Then, the workflow of the CAE methodology illustrated in Figure 3 is repeated for each retained set of values for the optimization weighting factors. Considering a population of 25 swarm particles, values for inertia, cognitive factor and social factor of 1, 5 and 2 respectively, and a maximum number of 10 iterations, around 2 to 3 hours are required to perform the workflow illustrated in Figure 3 using a desktop computer with Intel Core i7-8700 (3.2 GHz) and 32 GB of RAM. The implemented CAE methodology requires the synergic usage of two software with MATLAB® being responsible of managing the PSO workflow and parameters while launching numerical simulations in Amesim® software of the BEV embedding sizing candidates and performing reported braking maneuvers. An initial pedal force value of 500 N is retained for each simulated test. In case wheels lockup occurs, simulations of the same braking maneuver is repeated while gradually decreasing the brake pedal force. In case a brake pedal force value of 65 N is reached without satisfying the test constraints, the corresponding hydraulic brake system sizing candidate is marked as unfeasible and the following candidate is evaluated.

Both FWD and RWD cases are considered for the EM location in order to exhaustively compare overall BEV layout options both from energy and design points of view. For the sake of further comparison, an hydraulic brake system layout for the CV related to the specifications of Table 2 is simulated as well following the CAE workflow of figure 3. In this case, the electrically assisted brake booster is replaced with a traditional vacuum-assisted booster. Sizing parameters and numerical model for the vacuum-assisted booster are retained from [11]. The optimization target for the CV layout is represented by the overall size of the hydraulic brake system solely, since recovering the vehicle kinetic energy during braking is not possible. Obtained optimization results are plotted in figure 4 with $\overline{E_{batt}}$ and size cost function as independent variables.

In general, obtained Pareto frontiers suggest that, for both FWD and RWD cases, finding a global optimum for the hydraulic brake system sizing candidates considering the illustrated targets is not possible. Rather, a trade-off needs definition between the overall size of the system and the recovered electrical energy during braking. Table 4 and Table 5 report sizing and performance parameters for some sub-optimal results of obtained Pareto

Table 2 Vehicle specifications

Component	Parameter	Value
Vehicle body	Mass (GVWR)	1125 Kg
	h_{CoG} (GVWR)	525.5 mm
	a_{CoG} (GVWR)	1653.3 mm
	Mass (LLVW)	1450 Kg
	h_{CoG} (LLVW)	559.0 mm
	a_{CoG} (LLVW)	1180.9 mm
	Wheelbase	2550 mm
	Frontal area	2.37 m^2
EM	Maximum power	49 kW @ 2500-8000 rpm
	Maximum regenerative torque	180 Nm @ 0-2000 rpm
Trans-mission	Reduction gear ratio	6.066
Battery pack	Nominal voltage	330 V
	Capacity	16 kWh

Table 3 Retained values for sizing parameters

Parameter	Minimum value	Maximum value
Master cylinder diameter	12.7 mm	25.4 mm
Master cylinder stroke	33.25 mm	43.67 mm
Ratio d_{boost}/ d_{MC}	1	2.45
Front wheels brake piston diameter	28.58 mm	50.80 mm
Rear wheels brake piston diameter	28.58 mm	50.80 mm

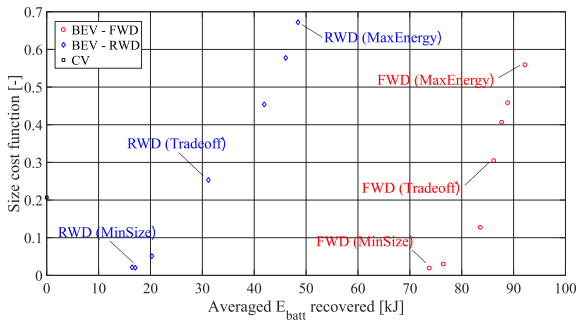

Figure 4 Simulation results

frontiers for FWD and RWD cases, respectively. With reference to figure 4, sizing candidates corresponding to the maximum recovered electrical energy, the minimum overall hydraulic brake system size and a trade-off between the two optimization targets are particularly reported and compared with the optimal CV brake system layout.

Results suggest that, from the energy point of view, a FWD BEV layout is more appealing than a RWD BEV layout. This relates to MinSize, MaxEnergy and TradeOff sub-optimal sizing candidates for FWD BEV achieving 4.48, 1.90 and 2.76 times the amount of electrical energy recovery compared with the RWD counterparts for the considered braking maneuvers. Results of this kind might reveal significant when selecting the EM location.

Concerning the master cylinder diameter, a 9.61 % reduction can be achieved for both RWD BEV and FWD BEV sub-optimal brake system layouts in terms of size compared with CV. Nevertheless, reducing the master cylinder diameter results in a higher brake line pressure and in turn friction torques, thus compromising the electrical energy recovery capability through the EM operation. To overcome this drawback, the PSO algorithm embedded in the developed CAE methodology appears increasing d_{MC} when optimizing predominantly for energy recovery. The master cylinder diameter indeed increases by 44.38 % and 44.68 % compared to its CV counterpart in FWD BEV and RWD BEV cases, respectively. When focusing on energy recovery, the sub-optimal brake system sizing candidates exhibit increased values for the master cylinder stroke as well. In this way, storing more fluid allows enhancing the friction braking capability at the non-driven wheels and preserving the energy recovery capability at the driven wheels. This particularly reveals effective for the RWD case, in which the EBD can reduce the brake line pressure at the rear wheels and let the EM operate more effectively. An increase of 13.43 % in st_{MC} can be observed in this case compared to the CV layout. On the other hand, the increase in st_{MC} appears mitigated when shifting from MinSize to MaxEnergy sub-optimal sizing candidates for the FWD BEV case.

As concerns the brake booster diameter, remarkable down-sizing can be obtained for BEVs compared to CVs through the adoption of a dedicated brake boosting technology. This can be correlated with the electrically assisted booster being capable of delivering consistent compression force in the master cylinder regardless of the hydraulic pressure generated. As example, a reduction of 93.21 % in d_{boost} can be achieved for MinSize sub-optimal results for both

Table 4 Results for CAE methodology - FWD

	CV	FWD (MinSize)	FWD (MaxEnergy)	FWD (Tradeoff)
d_{MC} [mm]	14.05	12.70	25.26	18.20
st_{MC} [mm]	38.50	33.25	37.05	33.28
d_{boost} [mm]	187	12.70	50.53	20.39
d_{BP_front} [mm]	30.43	28.58	25.58	28.58
d_{BP_rear} [mm]	28.58	28.58	42.79	47.15
Size cost	0.21	0.02	0.56	0.30
$\overline{E_{batt}}$ [kJ]	0	73.75	92.22	86.21

Table 5 Results for CAE methodology - RWD

	CV	RWD (MinSize)	RWD (MaxEnergy)	RWD (Tradeoff)
d_{MC} [mm]	14.05	12.70	25.40	16.36
st_{MC} [mm]	38.50	33.25	43.67	36.43
d_{boost} [mm]	187	12.70	56.80	16.67
d_{BP_front} [mm]	30.43	28.58	36.60	38.90
d_{BP_rear} [mm]	28.58	28.58	28.58	28.58
Size cost	0.21	0.02	0.67	0.25
$\overline{E_{batt}}$ [kJ]	0	16.46	48.44	31.16

FWD BEV and RWD BEV cases compared to CV, respectively. Considering MaxEnergy sub-optimal sizing candidates, these exhibit larger brake booster diameters to enhance the braking capability of the non-driven wheels as already explained for st_{MC}.

A well-established trend can then be observed for brake piston diameters, with the non-driven wheels exhibiting larger brake pistons with respect to the driven wheels. As example, for the MaxEnergy sub-optimal sizing candidates, the rear brake piston diameter increases the front brake piston diameter by 67.28 % for the FWD cases, while the front brake piston diameter increases the rear brake piston diameter by 28.06 % for the RWD case. Since values of brake piston diameters for the driven axle always correspond to the considered minimum, further down-sizing could be possible by including smaller values of brake piston diameters in the sizing space.

In general, the proposed CAE methodology allows effectively down-sizing hydraulic brake systems for electrified road vehicles. When optimizing while focusing on brake system size, the average size cost terms for both FWD BEV and RWD BEV cases reduce the CV counterpart by 90.48 %. On the other hand, when predominantly aiming at enhancing electrical energy recovery capabilities, $\overline{E_{batt}}$ for sub-optimal designs ameliorate the corresponding MinSize sub-optimal candidates by 25.04 % and 194.29 % for FWD and RWD cases, respectively. However, this

can be achieved at the expenses of upsizing the hydraulic brake system: the size cost terms for MaxEnergy sub-optimal layouts indeed increase the CV counterparts by 166.67 % and 219.05 % for FWD BEV and RWD BEV cases, respectively. In this framework, the identified trade-off sub-optimal sizing candidates might reveal suitable options in achieving good performance for both optimization targets simultaneously. However, it should be noted that the developed CAE methodology preserves the freedom of the brake system designer in choosing the appropriate hydraulic brake system sizing candidate according to their own decision criteria.

5. Conclusions

In this paper, a CAE methodology to appropriately size the hydraulic brake system of electrified road vehicles is illustrated. Numerical models for hydraulic brake system, BEV powertrain and vehicle chassis have been presented and implemented in Amesim® software.

A multi-target optimization framework is then considered in overall down-sizing the hydraulic brake system while maximizing the energy recovery capability of the BEV. A PSO algorithm is particularly adopted for selecting the right sizes of components, while the simulation of safety standard braking maneuvers ensures that only sizing candidates capable of complying with regulatory requirements are considered. The optimal Pareto frontier can then be obtained by repeating the optimization workflow while sweeping different weights for size cost term and energy cost term.

In general, the developed CAE methodology is proven effective at down-sizing hydraulic brake systems for electrified road vehicles. Nevertheless, it has been demonstrated here that excessively down-sizing the hydraulic brake system might compromise the electrical energy recovery capability of the electrified road vehicle in some operating conditions. For this reason, a flexible multi-objective optimization is performed to let brake system designers select the best sizing trade-off according to their decision criteria. Both FWD and RWD cases have been analyzed for a BEV layout. Despite the RWD layout might reveal more appealing due to enhanced acceleration capability, the FWD layout exhibits improved electrical energy recovery capability. On average, values of overall recovered battery electrical energy for the FWD BEV layout are indeed more than doubled with respect to the RWD counterpart.

Related future work might consider furtherly enhancing the model fidelity level for hydraulic brake systems [30]. Moreover, additional optimization criteria (e.g. lifetime, cost, wear) and electrified powertrain layouts might be considered. Finally, further braking maneuvers both from safety standards and real-world driving could be included in the proposed CAE methodology.

References

[1] B. Bilgin, P. Magne, P. Malysz, Y. Yang, V. Pantelic, M. Preindl, A. Korobkine, W. Jiang, M. Lawford, A. Emadi, "Making the Case for Electrified Transportation", *IEEE Transactions on Transportation Electrificatio*n, vol. 1, no. 1, pp. 4-17, 2015.

[2] P. G. Anselma, Y. Huo, J. Roeleveld, G. Belingardi and A. Emadi, "Integration of On-Line Control in Optimal Design of Multimode Power-Split Hybrid Electric Vehicle Powertrains," *IEEE Transactions on Vehicular Technology*, vol. 68, no. 4, pp. 3436-3445, 2019.

[3] P.G. Anselma, Y. Huo, J. Roeleveld, A. Emadi, G. Belingardi, "Rapid Optimal Design of a Multimode Power Split Hybrid Electric Vehicle Transmission", *Proceedings of the Institution of Mechanical Engineers, Part D: Journal of Automobile Engineering*, vol. 233, no. 3, pp. 740-762, 2019.

[4] P.G. Anselma, G. Belingardi, "Next generation HEV powertrain design tools: roadmap and challenges," *SAE Technical Paper* 2019-01-2602, 2019.

[5] Zhang, L., Yu, L., Pan, N., Zhang, Y., & Song, J. , "Cooperative control of regenerative braking and hydraulic braking of an electrified passenger car", *Proceedings of the Institution of Mechanical Engineers, Part D: Journal of Automobile Engineering*, vol. 226, no. 10, pp. 1289-1302, 2012.

[6] Z. Junzhi, L. Yutong, L. Chen, Y. Ye, "New regenerative braking control strategy for rear-driven electrified minivans", *Energy Conversion and Management*, vol. 82, pp. 165-145, 2014.

[7] Kumar, C. N., Subramanian, S. C., "Cooperative control of regenerative braking and friction braking for a hybrid electric vehicle", *Proceedings of the Institution of Mechanical Engineers, Part D: Journal of Automobile Engineering*, vol. 230, no. 1, pp. 103–116, 2015.

[8] Hall, T., "A Comparison of Braking Behavior between an IC Engine and Pure Electric Vehicle in Los Angeles City Driving Conditions," *SAE Technical Paper* 2017-01-2518, 2017.

[9] Shenberger, M. and Antanaitis, D., "Brake System Design for Dedicated BEV Architectures," *SAE Technical Paper* 2018-01-1870, 2018.

[10] P. G. Anselma, S. P. Patil and G. Belingardi, "Rapid design of a light vehicle hydraulic brake system," *2017 2nd IEEE International Conference on Intelligent Transportation Engineering (ICITE)*, Singapore, pp. 30-35, 2017.

[11] Anselma, P.G., Patil, S.P., and Belingardi, G., "Rapid Optimal Design of a Light Vehicle Hydraulic Brake System," *SAE Technical Paper* 2019-01-0831, 2019.

[12] Ohtani, Y., Innami, T., Obata, T., Yamaguchi, T. et al., "Development of an Electrically-Driven Intelligent Brake Unit," *SAE Technical Paper* 2011-01-0572, 2011.

[13] Goodarzi, A., Mehrmashhadi, J., and Esmailzadeh, E., "Optimised Braking Force Distribution Strategies for Straight and Curved Braking," *International Journal of Heavy Vehicle* Systems, vol. 16, no. 10, pp. 78-101, 2009.

[14] Mechanical Simulation, "Brake System with Boost and Thermal Effects", *CarSim Browser Reference Manual*, 2016.

[15] S. Heydari, P. Fajri, R. Sabzehgar and M. Rasouli, "A Novel Approach for Maximizing Regenerative Braking Energy Extraction of Electric Vehicles Using Motor Performance Lookup Table," *2019 IEEE Transportation Electrification Conference and Expo (ITEC)*, Detroit, MI, USA, 2019, pp. 1-5.

[16] M. T. Emırler, K. KahramanM. ŞentürkO. U. AcarB. Aksun GüvençL. GüvençB. Efendıoğlu, "Lateral stability control of fully electric vehicles", *International Journal of Automotive Technology*, vol. 16, no. 2, pp. 317-328, 2015.

[17] P.G. Anselma, G. Belingardi, "Comparing battery electric vehicle powertrains through rapid component sizing", *Int. J. Electric and Hybrid Vehicles*, vol. 11, no. 1, pp. 36–58, 2019.

[18] Pacejka H.B., Besselink I.J.M., "Magic formula tyre model with transient properties", *Proceeding of the 2nd Int. Colloquium on Tyre Models for Vehicle Dynamic Analysis*, Berlin, Germany, 1997, pp 234-249.

[19] Parsopoulos, Konstantinos E., and Michael N. Vrahatis. "Recent approaches to global optimization problems through

particle swarm optimization", *Natural computing*, vol. 1, nos. 2-3, pp. 235-306, 2002.

[20] E. Denimal, S. Nacivet , J J. Sinou, L. Nechak, "A strategy based on genetic algorithm to deal with influent internal contacts", *2018 FISITA Eurobrake*, The Hague, Netherlands, 2018.

[21] Nouiri, M., Bekrar, A., Jemai, A., Niar, S., and Ammari, A. C., "An effective and distributed particle swarm optimization algorithm for flexible job-shop scheduling problem", *Journal of Intelligent Manufacturing*, vol. 29, no. 3, pp. 603-615, 2018.

[22] R. Precup, M. Sabau, C. Dragos, M. Radac, L. Fedorovici and E. M. Petriu, "Particle Swarm Optimization of fuzzy models for Anti-Lock Braking Systems," *2014 IEEE Conference on Evolving and Adaptive Intelligent Systems (EAIS)*, Linz, Austria, 2014, pp. 1-6.

[23] Zhao, W., Yang, Z., and Wang, C., "Multi-objective optimization of chassis integrated system for electric wheel vehicle", *Proceedings of the Institution of Mechanical Engineers, Part C: Journal of Mechanical Engineering Science*, vol. 233, no. 1, pp. 7–17, 2019.

[24] Yarpiz, "Particle Swarm Optimization in MATLAB", [online] Available: https://yarpiz.com/50/ypea102-particle-swarm-optimization, accessed 10 Jan. 2020.

[25] U.S. Department of Transportation - NHTSA, "Federal Motor Vehicle Safety Standard No. 135; Light Vehicle Brake Systems," Dec 2, 2005. [Online] Available: https://www.nhtsa.gov/DOT/NHTSA/.../TP-135-01.pdf, accessed 10 Jan. 2020.

[26] Economic Commission for Europe, "Regulation No. 13-H - Uniform Provisions Concerning the Approval of Passenger Cars with Regard to Braking," Feb. 24, 2014. [Online] Available: https://www.unece.org/fileadmin/DAM/trans/doc/2007/wp29/ECE-TRANS-WP29-2007-03e.pdf , accessed 10 Jan. 2020.

[27] G. Wager, J. Whale, T. Braunl, "Performance evaluation of regenerative braking systems", *Proceedings of the Institution of Mechanical Engineers, Part D: Journal of Automobile Engineering*, vol. 232, no. 10, pp. 1414–1427, 2018.

[28] Mitsubishi, "MiEV Technical Specifications", [Online], Available: https://www.mitsubishi-motors.com/en/showroom/i-miev/specifications/, accessed 13 Jan. 2020.

[29] Dabadie, J., Sciarretta, A., Font, G., and Le Berr, F., "Automatic Generation of Online Optimal Energy Management Strategies for Hybrid Powertrain Simulation," *SAE Technical Paper* 2017-24-0173, 2017.

[30] Y. Yang, J. Zou, Y. Yang, D. Qin, "Design and Simulation of Pressure Coordinated Control System for Hybrid Vehicle Regenerative Braking System", *J. Dyn. Sys., Meas., Control*, vol. 136, no. 5, pp. 1-8, 2014.